Materials Chemistry and Physics 180 (2016) 213–218

Contents lists available at ScienceDirect

Materials Chemistry and Physics

journal homepage: www.elsevier.com/locate/matchemphys

Lattice dynamics and anharmonicity of $CaZrF_6$ from Raman spectroscopy and *ab initio* calculations

Andrea Sanson [a, *], Marco Giarola [b], Gino Mariotto [b], Lei Hu [c], Jun Chen [c], Xianran Xing [c]

[a] Department of Physics and Astronomy, University of Padova, Padova, Italy
[b] Department of Computer Science, University of Verona, Verona, Italy
[c] Department of Physical Chemistry, University of Science and Technology Beijing, Beijing, China

HIGHLIGHTS

- A Raman and *ab initio* study of the lattice dynamics of $CaZrF_6$ was performed.
- All the Raman-active modes expected on the basis of the group theory were identified.
- The temperature-dependence of the $CaZrF_6$ Raman frequencies follows an unusual trend.
- Explicit anharmonicity dominates for both F_{2g} and A_g Raman modes.
- The NTE of $CaZrF_6$ cannot be accurately predicted by the quasi-harmonic approximation.

GRAPHICAL ABSTRACT

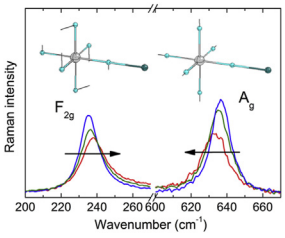

ARTICLE INFO

Article history:
Received 18 January 2016
Received in revised form
23 May 2016
Accepted 30 May 2016
Available online 7 June 2016

Keywords:
Thermal expansion
Raman spectroscopy and scattering
Lattice dynamics
Anharmonicity

ABSTRACT

Very recently it has been found that $CaZrF_6$ exhibits a very large and isotropic negative thermal expansion (NTE), even greater than the current most popular NTE materials. In this work, the vibrational dynamics of $CaZrF_6$ has been investigated by temperature-dependent Raman spectroscopy combined with *ab initio* calculations. As expected on the basis of the group theory for $CaZrF_6$, three Raman-active modes were identified: the F_{2g} mode peaked at about 236 cm^{-1}, the E_g mode at around 550–555 cm^{-1}, and the A_g mode peaked at about 637 cm^{-1}. The temperature dependence of their frequencies follows an unusual trend: the F_{2g} mode, due to bending vibrations of fluorine atoms in the linear Ca-F-Zr chain, is hardened with increasing temperature, while the A_g mode, corresponding to Ca-F-Zr bond stretching vibrations, is softened. We explain this anomalous behavior by separating implicit and explicit anharmonicity for both F_{2g} and A_g modes. In fact, cubic anharmonicity (three-phonon processes) is observed to dominate the higher-frequency A_g phonon-mode, quartic anharmonicity (four-phonon processes) is found to dominate the lower-frequency F_{2g} phonon-mode. As a result, the large NTE of $CaZrF_6$ cannot be accurately predicted through the quasi-harmonic approximation.

1. Introduction

Most materials expand upon heating. In the last two decades, after the discovery of materials that display strong negative thermal expansion (NTE) over wide temperature ranges, such as ZrW_2

* Corresponding author.
E-mail address: andrea.sanson@unipd.it (A. Sanson).

http://dx.doi.org/10.1016/j.matchemphys.2016.05.067
0254-0584/

O_8, $Zn(CN)_2$, metal-organic frameworks and more recently ScF_3 [1–6], the interest in NTE has rapidly increased. NTE phenomenon is known to arise from a range of different physical mechanisms, such as ferroelectricity and magnetic transitions [7–9], valence transitions in the case of intermetallic and fulleride materials [10,11], low-energy vibrational modes for open-framework solids [12–15]. In particular, it is now accepted that the mechanism driving NTE in the framework structures involves transverse vibrational displacement of the central linking atom [13–16], but a general understanding of the physical origin of NTE (and related phenomena) is still lacking.

Very recently it has been discovered that $CaZrF_6$ displays a very large and isotropic NTE (up to -18×10^{-6} K^{-1} at 100 K) [18], even greater than the current most popular NTE materials like ZrW_2 O_8 or ScF_3. In addition, the NTE temperature range of $CaZrF_6$ ranges from below 10 K–1173 K or even higher, thus making this material until now the one with the largest NTE temperature range. Besides this, $CaZrF_6$ is transparent over a wide wavelength range, can be fabricated in ceramic form and handled in air, thus being beneficial for the design of controlled thermal expansion materials and for technological applications.

From the structural point of view, $CaZrF_6$ consists of corner-shared CaF_6 and ZrF_6 octahedra (Fig. 1) and maintains a high symmetry (space group, Fm-3m) among the whole temperature range. In sharp contrast with ZrW_2 O_8, no phase transition takes place in $CaZrF_6$. Besides, the metal atoms both locate in the special crystallographic sites (Ca (0,0,0) and Zr (0.5,0.5,0.5)) and all the fluorine atoms share the same chemical environment. The prevailing NTE characteristic and its high cubic symmetry structure enable $CaZrF_6$ to be an excellent candidate for the study of NTE mechanism, whose knowledge would facilitate the development of specifically tailored materials based on a priori knowledge rather than empirical or casual procedures.

Because very limited information are available concerning the vibrational properties of $CaZrF_6$ and, even better, about its NTE mechanism, in this work we aim to investigate the lattice dynamics of $CaZrF_6$ by temperature-dependent Raman scattering combined with *ab initio* calculations. Raman spectroscopy only probes zone center modes thus providing a limited view of the lattice dynamics, nevertheless we can get new insights into the vibrational dynamics of $CaZrF_6$ related to the NTE.

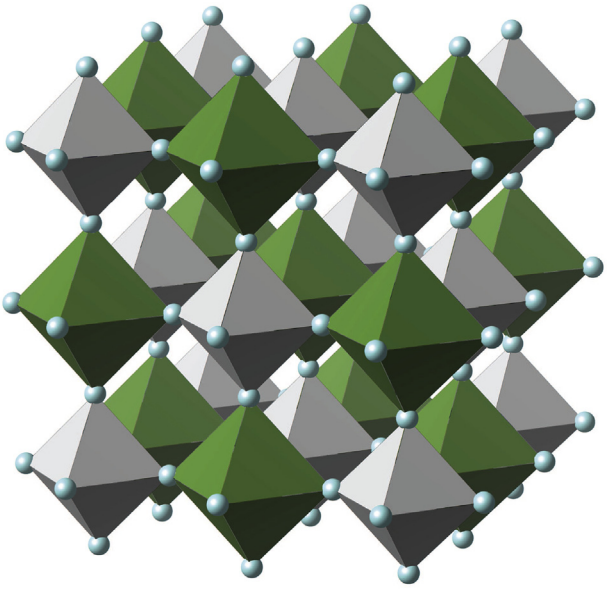

Fig. 1. Sketch of the crystal structure of $CaZrF_6$[17]: gray and green octahedra are ZrF_6 and CaF_6 units, respectively, cyan spheres are fluorine atoms. (For interpretation of the references to colour in this figure legend, the reader is referred to the web version of this article.)

2. Experimental and computational details

The compound of $CaZrF_6$ was prepared by a solid state synthesis method. The precursors of high purity (99.99%) CaF_2 and ZrF_4 powders, were mixed with equal molar ratio. Then the mixture was pressed into a small pellet with diameter of ~ 5 mm and then sandwiched into NH_4 F powder to be pressed into a bigger one with diameter of ~ 10 mm. The pellet was loaded into Cu tube with two ends sealed and transferred to a muffle furnace immediately, followed by heating them at 700 °C for 1 h, before they were slowly decreased to room temperature. Lab X-ray powder diffraction (XRD) data of $CaZrF_6$ was collected at room temperature, operating at 40 kV and 40 mA with Cu $K\alpha_{1/2}$ radiation (PANalytical, PW 3040-X'Pert Pro). The XRD data shows that the main phase is $CaZrF_6$ with an extremely tiny amount of ZrO_2 impurities in monoclinic phase (Fig. 2). Structural refinement gives a lattice parameter of 8.4630 Å with fluorine cell position $x = 0.2366$, in agreement with Hancock et al. [18].

Unpolarized micro-Raman spectra were collected in backscattering geometry from $CaZrF_6$ sample using a triple monochromator (Horiba-Jobin Yvon, model T64000), set in double-subtractive/single configuration, and equipped with holographic gratings having 1800 lines/mm. The Raman spectra were excited by the 514.5 nm laser line focused onto a spot of about 2 μm in size through the lens of a 50 × microscope objective (NA = 0.5). The laser power on the sample surface was kept below 10 mW, and the scattered radiation, filtered by the fore double monochromator, was detected at the spectrograph output by a charge-coupled-device detector with 1024 × 256 pixels, cooled by liquid nitrogen. The spectral resolution was better than 0.6 cm^{-1}/pixel while an accurate wave-number calibration of the spectrometer was achieved based on the emission lines of a Ne spectral lamp. The temperature dependence of the Raman spectra of $CaZrF_6$ was investigated in the temperature range between room temperature and 200 °C with the use of an electric heating plate.

Ab initio calculations based on density functional theory in the framework of local density approximation have been performed to calculate the Raman active vibrational modes of $CaZrF_6$. This

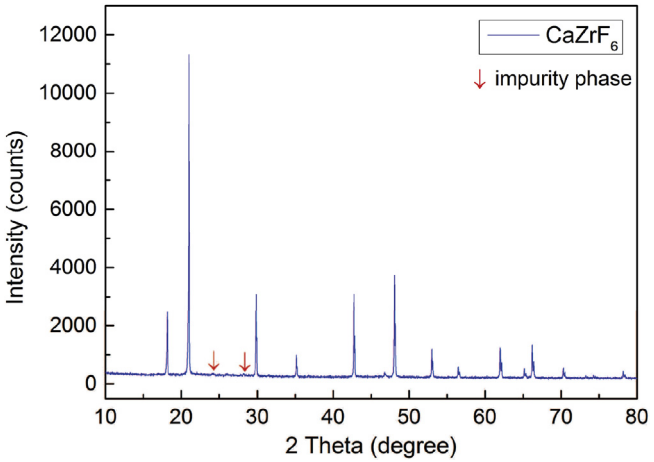

Fig. 2. X-ray diffraction pattern of $CaZrF_6$ with a tiny amount of ZrO_2 impurity marked by red arrows. (For interpretation of the references to colour in this figure legend, the reader is referred to the web version of this article.)

represents an invaluable help for the assignment of the observed Raman modes. The CRYSTAL-14 package was used in the present calculations, a periodic *ab initio* code that uses a Gaussian-type basis set to represent the crystalline orbitals [19]. All-electron basis sets were employed, with 86-511d3G contraction (one s, four sp, and one d shell) for calcium [20], 97-636121 contraction (one s, three sp, one d, one sp, and two d shells) for zirconium [21], and with 7-311G contraction (one s and three sp shells) for fluorine [22]. Pure density functional theory calculations have been carried out using von Barth-Hedin [23] exchange and correlation functionals. The Brillouin zone was sampled by a 12 × 12 × 12 Monkhorst-Pack k-points mesh [24], while the truncation criteria for bi-electronic integrals (Coulomb and exchange series), controlled by five parameters, was set to default values (7 7 7 7 14). In order to ensure good convergence, the self-consistent-field convergence threshold on total energy was set to 10^{-8} Hartree for geometry optimization, to 10^{-10} Hartree for frequency calculation. The vibrational frequencies at the Γ-point of the Brillouin zone were calculated in the harmonic approximation by diagonalizing the mass-weight Hessian matrix, whose (i,j) element is defined as $W_{ij} = H_{ij}/M_iM_i$, with M_i and M_j masses of the ith and jth atoms, respectively. A more detailed description of the computational aspects can be found in the refs. [19,25,26].

3. Results and discussion

On the basis of the group factor analysis, 21 optical modes of $CaZrF_6$ at the Γ-point of the Brillouin zone are expected, with the following irreducible representation of the normal vibrational modes:

$$3F_{1u} + 1F_{2u} + 1F_{2g} + 1F_{1g} + 1E_g + 1A_g \quad (1)$$

where the F_{1u}, F_{2u}, F_{1g} and F_{2g} modes are triple degenerated, the E_g mode is double degenerated. The three modes F_{2g}, E_g and A_g are Raman active, whereas the three F_{1u} modes are infrared active and the remaining F_{1u} and F_{1g} modes are inactive (silent). In order to discriminate the Raman F_{2g}, E_g and A_g modes, it would be necessary to control the polarization direction of the incident and scattered light with respect to the crystallographic axes. However this is impossible in our powder sample because no crystallographic axis can be identified. Accordingly, for the assignment of the observed Raman modes, we have calculated the vibrational frequency of the Raman-active modes through *ab initio* quantum-mechanical methods (see below).

The unpolarized Raman spectrum collected in our $CaZrF_6$ sample at room temperature is shown in the top panel of Fig. 3. Two intense Raman bands are observed at about 236 and 637 cm^{-1}, as well as a broad band at about 550–555 cm^{-1}. Moreover, we notice a set of weak Raman bands at ~179, 191, 324, 348, 384, and 475 cm^{-1}, marked by asterisk in the top panel of Fig. 3, which correspond to the Raman peak positions of monoclinic ZrO_2 [27,28], tiny impurity in the sample previously detected by x-ray diffraction (Fig. 2). In this regard, under direct optical inspection of a color camera interfaced to the microscope objective used to collect the scattered radiation, we have identified in the sample a grain of ZrO_2 impurity

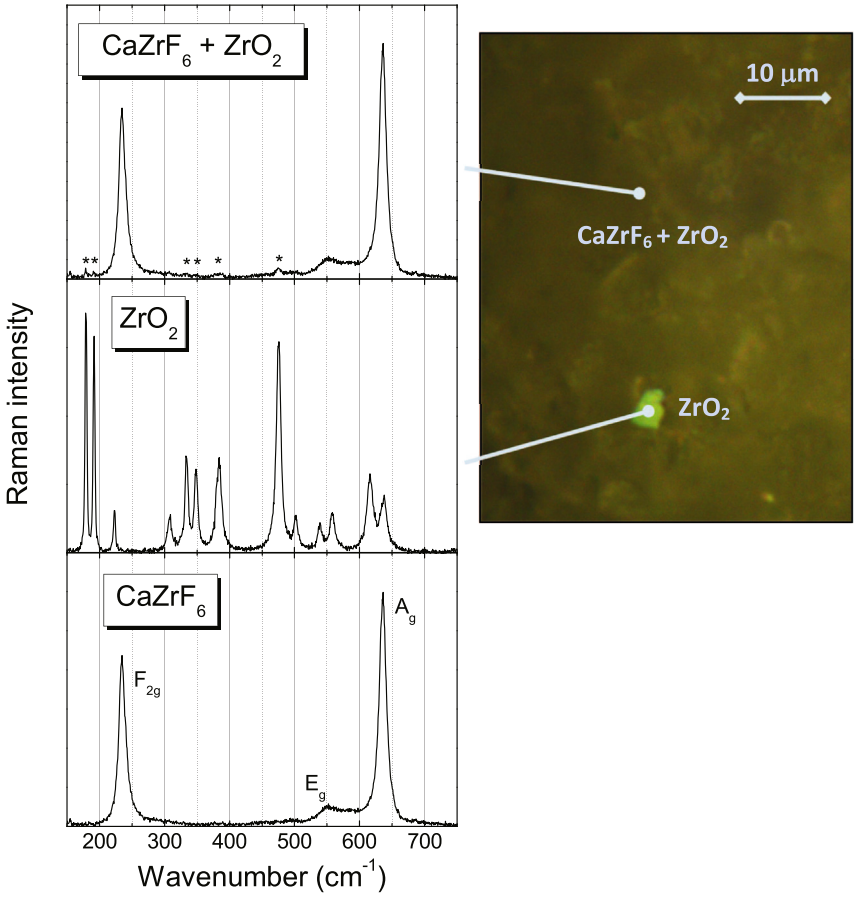

Fig. 3. Room temperature unpolarized Raman spectrum of: *i*) $CaZrF_6$ with a tiny amount of ZrO_2 impurity (top panel, the asterisks mark the most intense Raman peaks of ZrO_2) *ii*) a grain of ZrO_2 impurity identified in the sample (middle panel and picture on the right side) *iii*) $CaZrF_6$ after partial removal of the ZrO_2 Raman contribution (bottom panel).

Table 1
Observed and calculated vibrational frequencies of $CaZrF_6$ (in cm^{-1}) at the Γ-point of Brillouin zone. The Grüneisen parameters $\gamma_i = -V/\omega_i(\partial\omega_i/\partial V)$ of each vibrational mode were calculated by pressure-dependent *ab initio* calculations (see text).

Modes	Expt.	Theory	γ_i
Raman modes			
F_{2g}	236	251	−0.36
E_g	~550	529	1.69
A_g	637	637	1.26
Infrared modes			
F(1)1*u*		193	−1.83
F(2)1*u*		313	2.10
F(3)1*u*		542	1.68
Silent modes			
F_{1g}		41	−34.9
F_{2u}		117	−3.41

(picture in Fig. 3) whose Raman spectrum is reported in the middle panel of Fig. 3. Then, after proper normalization, the Raman contribution of ZrO_2 has been subtracted, thus obtaining the Raman spectrum of $CaZrF_6$ shown in bottom panel of Fig. 3.

Theoretical calculations help to assign the observed Raman peaks of $CaZrF_6$ and to gain further insight into its vibrational properties. First of all, geometry optimization was performed leading to the cell parameter $a = 8.4260$ Å and to the fluorine cell position $x = 0.2389$. These structural parameters, which differ from the experimental values less than 1.0%, have been employed in the subsequent frequency calculation. Table 1 shows the predicted vibrational frequencies of $CaZrF_6$ at the Γ-point of the Brillouin zone. To the best of our knowledge, no experimental data are available for both Raman and infrared vibrational modes of $CaZrF_6$, with the exception of the present Raman study. Thanks to the direct comparison between calculated and experimental frequencies (see Table 1), we can identify the Raman bands of $CaZrF_6$ shown in Fig. 3. Specifically, the Raman band observed at ~236 cm^{-1} is assigned to the F_{2g} symmetry mode, the band at ~550 cm^{-1} corresponds to the E_g symmetry mode, the band at ~637 cm^{-1} is the A_g symmetry mode. From the eigenvectors analysis (Fig. 4), the F_{2g} vibrational mode corresponds to bending vibrations of fluorine atoms perpendicular to the linear Zr-F-Ca bonds, leading to twisting of the ZrF_6 and CaF_6 octahedra. Instead the E_g and A_g vibrational modes correspond, respectively, to the asymmetric and symmetric stretching of the Zr-F and Ca-F bonds in the ZrF_6 and CaF_6 octahedra. In particular, the A_g mode is a breathing mode, as depicted in Fig. 4.

Temperature dependence of vibrational modes plays a key role for the negative thermal expansion of $CaZrF_6$. For that reason, we have investigated the temperature dependence of the frequency of the F_{2g} and A_g modes in the Raman spectra of $CaZrF_6$, from room temperature to about 200 °C. The same quantitative analysis cannot be done for the E_g Raman band because of its broadening and weak intensity.

The top panel of Fig. 5 shows the Raman shift of the F_{2g} and A_g vibrational bands at three selected temperatures, while the bottom panel of the same figure shows the resulting temperature dependence of the vibrational frequencies. It is surprising to observe that the F_{2g} mode, which is due to transverse vibrations and hence should be related to NTE, shows anomalous phonon hardening with increasing temperature. On the contrary the A_g mode, assigned to stretching vibrations, undergoes a phonon softening with temperature. This is exactly the opposite of what one would expect, since the transverse vibrations (here the F_{2g} mode), responsible for NTE, should display phonon softening with contracting crystal lattice, i.e., with temperature increasing.

To explain this anomalous behavior, we need to consider that the temperature dependent shift $\Delta\omega(T)$ of phonon frequency at constant pressure has two different contributions [29–31]: *i*) phonon frequency change $\Delta\omega_{vol}(T)$ due to volume expansion, which is the "quasi-harmonic" contribution also called "implicit" anharmonicity, and *ii*) "explicit" or "true" anharmonic contribution $\Delta\omega_{anh}(T)$, which is the pure-temperature effect due to anharmonic phonon-phonon interactions, arising from cubic, quartic, and higher-order anharmonic terms in the interatomic potential. Therefore

$$\Delta\omega(T) = \Delta\omega_{vol}(T) + \Delta\omega_{anh}(T) \tag{2}$$

For an isotropic system, equation (2) in differential form becomes

$$\left(\frac{\partial\omega_i}{\partial T}\right)_p = \left(\frac{\partial\omega_i}{\partial V}\right)_T \left(\frac{\partial V}{\partial T}\right)_p + \left(\frac{\partial\omega_i}{\partial T}\right)_V \tag{3}$$

which can also be written as

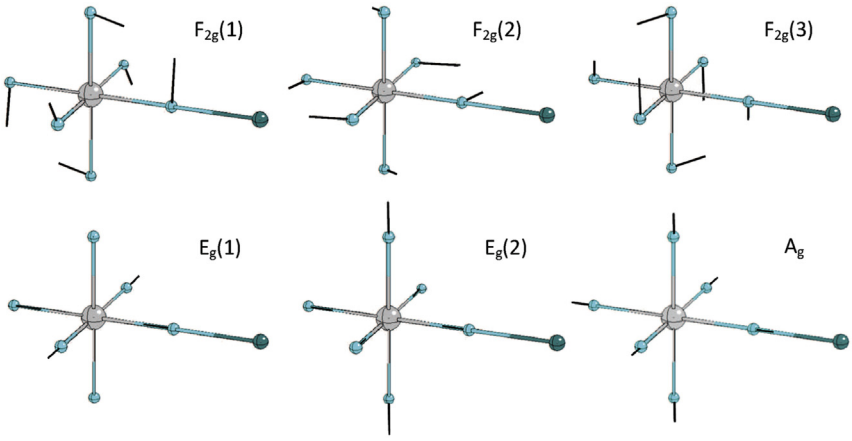

Fig. 4. Eigenvectors of the triple-degenerate F_{2g} mode, of the double-degenerate E_g mode, and of the A_g mode (gray, green and cyan spheres represent Zr, Ca and F atoms, respectively). The F_{2g} mode corresponds to bending vibrations of fluorine atoms perpendicular to the Zr-F-Ca bonds, leading to twisting of the ZrF_6 and CaF_6 octahedra. The E_g and A_g modes are, respectively, asymmetric and symmetric stretching of the Zr-F and Ca-F bonds in the ZrF_6 and CaF_6 octahedra. In particular, the A_g mode corresponds to a breathing mode. (For interpretation of the references to colour in this figure legend, the reader is referred to the web version of this article.)

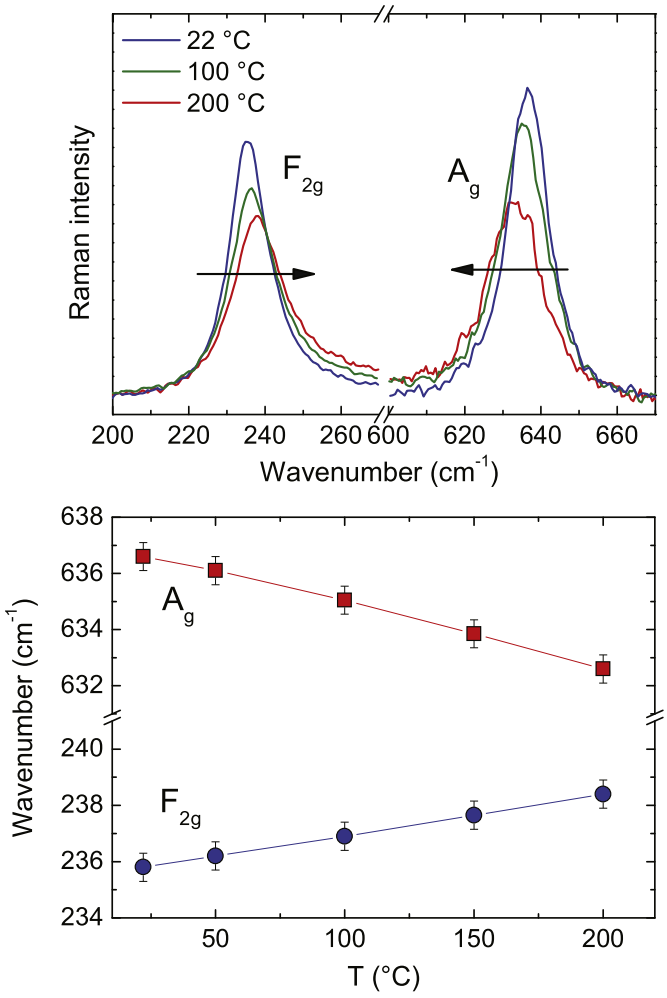

Fig. 5. Top panel: Raman shift of the F_{2g} and A_g vibrational bands at three selected temperatures. Bottom panel: temperature dependence of the vibrational frequency of the F_{2g} and A_g modes.

$$\frac{1}{\omega_i}\left(\frac{\partial\omega_i}{\partial T}\right)_p = -\alpha\gamma_i + \frac{1}{\omega_i}\left(\frac{\partial\omega_i}{\partial T}\right)_V \quad (4)$$

where α is the coefficient of linear thermal expansion and γ_i is the isothermal Grüneisen parameter for the vibrational mode ω_i. The term on the left-hand side of equation (4) gives the temperature-dependent frequency shift due to the total anharmonicity, as measured by temperature-dependent Raman spectra of Fig. 5. The first term on the right-hand side is the implicit anharmonicity due to volume contribution and can be determined from pressure-dependent frequency measurements and thermal expansion. The second term on the right-hand side is the explicit/true anharmonicity and cannot be determined experimentally. The temperature dependence of the F_{2g} and A_g Raman modes shown in Fig. 5 is the result of the balance between implicit and explicit anharmonicity.

In order to separate implicit and explicit anharmonicity for the F_{2g} and A_g modes, we have calculated the total anharmonicity (Table 2) from the temperature-dependence of the Raman frequencies shown in the bottom panel of Fig. 5. The implicit anharmonicity has instead been estimated by thermal expansion ($\alpha \simeq -11.5 \times 10^{-6}$ K^{-1} at 300 K [18]) and Grüneisen parameters γ_i, the latter obtained by pressure-dependent *ab initio* calculations performed in the pressure range from 0 to 300 MPa, corresponding to a reduction in lattice constant of about 0.15%. The resulting Grüneisen parameters for each vibrational modes at the Brillouin zone center are listed in the last column of Table 1, while the implicit anharmonic contribution of the F_{2g} and A_g Raman-active modes are reported in Table 2.

Firstly we find negative Grüneisen parameters for the lower-frequency modes (Table 1), in particular for the lowest-frequency F_{1g} symmetry mode corresponding to rigid rotation of CaF_6 and ZrF_6 octahedra around Ca and Zr, respectively, whose Grüneisen parameter is about −35. These findings are in agreement with the work of Hancock and co-workers [18] in which the most strongly negative Grüneisen parameters were associated with modes below ~150 cm^{-1}; furthermore, the large negative Grüneisen parameter of the F_{1g} mode indicates that rigid unit mode (RUM) mechanism [33,34] strongly contributes to the NTE in $CaZrF_6$. Note that typically the RUMs are optically active modes, like in ZrW_2O_8 [31,32], whereas in $CaZrF_6$ RUMs are silent due to the higher crystal symmetry. The linear thermal expansion coefficient α of $CaZrF_6$ at room temperature, calculated from the Grüneisen parameters listed in Table 1 (the reported value [18] of bulk modulus B=37 GPa is used in the calculation), is $\sim -2.3\times10^{-5}$ K^{-1} versus an experimental value of $\sim -11.5\times10^{-6}$ K^{-1} [18]. Obviously there is an inherent limit in this thermal expansion calculation since the modes in Table 1 are only a fraction of the entire Brillouin zone.

Secondly, the explicit/true anharmonicity of the F_{2g} and A_g Raman-active modes of $CaZrF_6$ has been determined by equation (4). As reported in Table 2, for both the F_{2g} and A_g modes the explicit anharmonic contribution is dominant over the implicit one. In addition, because the cubic anharmonic term leads to a decrease in frequency and, on the contrary, the quartic anharmonic term produces an increase in frequency [29,30], we can infer that cubic anharmonicity (i.e., three-phonon scattering processes) is dominant in the A_g phonon-mode, while the quartic anharmonicity (i.e., four-phonon scattering processes) is dominant in the F_{2g} phonon-mode. We should mention here that also in cubic ScF_3, which has the same ReO_3-type connectivity of $CaZrF_6$, there are a substantial number of modes with dominant quartic anharmonicty that accounts for phonon stiffening with temperature and for a significant part of the NTE [35,36]. As a result, the (negative) thermal expansion of $CaZrF_6$ cannot be fully explained in the framework of quasi-harmonic approximation.

4. Conclusions

The vibrational dynamics of NTE material $CaZrF_6$ has been

Table 2
Anharmonic contributions (in 10^{-5} K^{-1}) to the F_{2g} and A_g vibrational modes of $CaZrF_6$. The total anharmonicity has been determined from the temperature-dependence of the Raman frequencies shown in Fig. 5, the implicit anharmonicity has been estimated by pressure-dependent *ab initio* calculations and thermal expansion. The resulting explicit anharmonicty, separated using Eq. (4), indicates cubic anharmonicity (three-phonon processes) for the A_g mode and quartic anharmonicity (four-phonon processes) for the F_{2g} mode.

Modes	Total anharmonicity $1/\omega_i(\partial\omega_i/\partial T)_p$	Implicit anharmonicity $-\alpha\gamma_i$	Explicit anharmonicity $1/\omega_i(\partial\omega_i/\partial T)_V$
F_{2g}	6.18	−0.42	6.60
A_g	−3.81	1.45	−5.26

investigated by temperature-dependent Raman spectroscopy and *ab initio* calculations. The three expected Raman-active modes for $CaZrF_6$ have been reported for the first time. More interestingly, the vibrational frequency of the F_{2g} and A_g Raman modes, related to Ca-F-Zr bending and stretching vibrations, respectively, exhibit an anomalous dependence on temperature - exactly the opposite of what one would expect from the quasi-harmonic approximation. In order to shed light on this issue, we have separated implicit and explicit anharmonicity by means of pressure-dependent *ab initio* calculations. We have found out that explicit anharmonicity dominates over implicit anharmonicity, and the lower-frequency F_{2g} mode has significant quartic anharmonicity, while the higher-frequency A_g mode has significant cubic anharmonicity. The strong contribution of the explicit anharmonicity indicates that the large NTE of $CaZrF_6$ cannot be accurately predicted through the quasi-harmonic approximation.

References

[1] T.A. Mary, J.S.O. Evans, T. Vogt, A.W. Sleight, Science 272 (1996) 90.
[2] P. Badrinarayanan, M.I. Ahmad, M. Akinc, M.R. Kessler, Mater. Chem. Phys. 131 (2011) 12.
[3] A.L. Goodwin, C.J. Kepert, Phys. Rev. B 71 (2005) 140301 (R).
[4] K.W. Chapman, P.J. Chupas, C.J. Kepert, J. Am. Chem. Soc. 127 (2005) 15630.
[5] W. Zhou, H. Wu, T. Yildirim, J.R. Simpson, A.R.H. Walker, Phys. Rev. B 78 (2008) 054114.
[6] B.K. Greve, K.L. Martin, P.L. Lee, P.J. Chupas, K.W. Chapman, A.P. Wilkinson, J. Am. Chem. Soc. 132 (2010) 15496.
[7] J. Chen, K. Nittala, J.S. Forrester, J.L. Jones, J. Deng, R. Yu, X. Xing, J. Am. Chem. Soc. 133 (2011) 11114.
[8] J. Chen, L. Fan, Y. Ren, Z. Pan, J. Deng, R. Yu, X. Xing, Phys. Rev. Lett. 110 (2013) 115901.
[9] P. Mohn, Nature 400 (1999) 18.
[10] J.R. Salvador, F. Gu, T. Hogan, M.G. Kanatzidis, Nature 425 (2003) 702.
[11] J. Arvanitidis, K. Papagelis, S. Margadonna, K. Prassides, A.N. Fitch, Nature 425 (2003) 599.
[12] G. Ernst, C. Broholm, G.R. Kowach, A.P. Ramirez, Nature 396 (1998) 147.
[13] A. Sanson, F. Rocca, G. Dalba, P. Fornasini, R. Grisenti, M. Dapiaggi, G. Artioli, Phys. Rev. B 73 (2006) 214305.
[14] A. Sanson, Chem. Mater 26 (2014) 3716.
[15] J. Chen, L. Hu, J. Deng, X. Xing, Chem. Soc. Rev. 44 (2015) 3522.
[16] L. Wang, P.F. Yuan, F. Wang, Q. Sun, Z.X. Guo, E.J. Liang, Y. Jia, Mater. Chem. Phys. 148 (2014) 214.
[17] T.C. Ozawa, S.J. Kang, J. Appl. Cryst. 37 (2004) 679.
[18] J.C. Hancock, K.W. Chapman, G.J. Halder, C.R. Morelock, B.S. Kaplan, L.C. Gallington, A. Bongiorno, C. Han, S. Zhou, A.P. Wilkinson, Chem. Mater 27 (2015) 3912.
[19] R. Dovesi, R. Orlando, A. Erba, C.M. Zicovich-Wilson, B. Civalleri, S. Casassa, L. Maschio, M. Ferrabone, M. De La Pierre, P. DArco, Y. Noel, M. Causa, M. Rerat, B. Kirtman, Int. J. Quantum Chem. 114 (2014) 1287.
[20] M. Catti, R. Dovesi, A. Pavese, V.R. Saunders, J. Phys. Cond. Matter 3 (1991) 4151.
[21] R. Dovesi et al., http://www.crystal.unito.it/Basis_ Sets/zirconium.html (unpublished).
[22] R. Nada, C.R.A. Catlow, C. Pisani, R. Orlando, Model. Simul. Mater. Sci. Eng. 1 (1993) 165.
[23] U. von Barth, L. Hedin, J. Phys. C. Solid State Phys. 5 (1972) 1629.
[24] H.J. Monkhorst, J.D. Pack, Phys. Rev. B 13 (1976) 5188.
[25] F. Pascale, C.M. Zicovich-Wilson, F.L. Gejo, B. Civalleri, R. Orlando, R. Dovesi, J. Comput, Chem. 25 (2004) 888.
[26] C.M. Zicovich-Wilson, F. Pascale, C. Roetti, V.R. Saunders, R. Orlando, R. Dovesi, J. Comput, Chem. 25 (2004) 1873.
[27] B.K. Kim, H. Hamaguchi, Phys. Stat. Sol.(b) 203 (1997) 557 (and references therein).
[28] P.E. Quintard, P. Barbéris, A.P. Mirgorodsky, T. Merle-Méjean, J. Am. Ceram. Soc. 85 (2002) 1745.
[29] G. Lucazeau, J. Raman Spectr. 34 (2003) 478.
[30] N.P. Salke, M.K. Gupta, R. Rao, R. Mittal, J. Deng, X. Xing, J. Appl. Phys. 117 (2015) 235902.
[31] T.R. Ravindran, A.K. Arora, T.A. Mary, Phys. Rev. B 67 (2003) 064301.
[32] T.R. Ravindran, A.K. Arora, T.A. Mary, J. Phys. Cond. Matter 13 (2001) 11573.
[33] J.Z. Tao, A.W. Sleight, J. Sol. State Chem. 173 (2003) 442.
[34] M.T. Dove, K.O. Trachenko, M.G. Tucker, D.A. Keen, Rev. Mineral. Geochem 39 (2000) 1.
[35] C.W. Li, X. Tang, J.A. Munõz, J.B. Keith, S.J. Tracy, D.L. Abernathy, B. Fultz, Phys. Rev. Lett. 107 (2011) 195504.
[36] P. Lazar, T. Bučko, J. Hafner, Phys. Rev. B 92 (2015) 224302.